Annihilation dynamics of topological monopoles on a fiber in nematic liquid crystals

M. Nikkhou,[1] M. Škarabot,[1] and I. Muševič[1,2]
[1]*J. Stefan Institute, Jamova 39, SI-1000 Ljubljana, Slovenia*
[2]*Faculty of Mathematics and Physics, University of Ljubljana, Jadranska 19, SI-1000 Ljubljana, Slovenia*
(Received 18 January 2016; revised manuscript received 22 April 2016; published 13 June 2016)

We use the laser tweezers to create isolated pairs of topological point defects in a form of radial and hyperbolic hedgehogs, located close and attracted to a thin fiber with perpendicular surface orientation of nematic liquid crystal molecules in a thin planar nematic cell. We study the time evolution of the interaction between the two monopoles by monitoring their movement and reconstructing their trajectories and velocities. We find that there is a crossover in the pair interaction force between the radial and hyperbolic hedgehog. At small separation d, the elastic force between the opposite monopoles results in an increase of the attractive force with respect to the far field, and their relative velocity v scales as a $v(d) \propto d^{-2\pm0.2}$ power law. At large separations, the two oppositely charged monopoles can either attract or repel with constant interaction force. We explain this strange far-field behavior by the experimental inaccuracy in setting the fiber exactly perpendicular to the cell director.

DOI: 10.1103/PhysRevE.93.062703

I. INTRODUCTION

Topological properties of nematic liquid crystals with colloidal inclusions have attracted great interest in recent years due to the fascinating variety of observed phenomena and ease of observation and manipulation under an optical microscope. Whereas, over many years, the study of topological defects was limited to simple observations under an optical microscope by using simple means of analysis of their structure [1–10], modern techniques of defect manipulation and analysis have triggered a revival in this field during the past 10 years. New experimental techniques have been introduced to this field, such as the laser tweezers for particle and defect manipulation [11–25] and fluorescent confocal polarizing microscopy (FCPM) [26–28] for defect visualization and analysis. They allow for well-controlled studies of colloidal pair interactions in nematic and chiral nematic liquid crystals (NLCs) and 3D analysis of director structure. Laser tweezers have been used to assemble [29–35] and entangle various colloidal crystals and superstructures in NLCs [36], and knotted and linked colloidal structures [37,38] have been discovered and analyzed for the first time. Complex topological defects, such as disclinations in cholesteric wedges [28], torons [39], and Hopfions [40] in frustrated chiral NLCs, were studied and visualized using FCPM.

The dynamics and annihilation of topological defects has been for many years the subject of intensive experimental [41–48] and theoretical studies [49–52]. Defects are created either by a rapid temperature or pressure quench. To maintain the conservation of the total topological charge, the disclinations or point defects appear in pairs with opposite topological charges. Because of the inhomogeniety and elastic distortions of the director field around each defect, a structural force is generated, which attracts both defects until they meet and annihilate into the vacuum. Annihilation of point monopoles (hedgehogs) in the nematic liquid crystal was first observed in cylindrical capillaries by Williams *et al.* [53] and studied in detail by Pargellis *et al.* [42]. In thin nematic layers with hybrid surface alignment (homeotropic on one side and degenerate planar at the other side), Lavrentovich and Rozhkov [43] and Rapini *et al.* [44] studied the pair interaction of surface point defects called boojums (half monopoles attached to the surface), connected with strings of a deformed nematic liquid crystal. This was followed by many other studies, discussed further in this article.

Because the topological defects are entities moving within a liquid, the hydrodynamics of their motion plays an important role in the dynamics of their annihilation. There is a reorientation of the director field during the motion of defects, which is coupled to the flow of the liquid crystal. This coupling between the director field and velocity field results in the backflow, which has a substantial effect on the motion of defects and induces the asymmetry in their dynamics for different topological charges [50–54]. Both the experiments and theory show that the $+1/2$ winding number defects are always faster than the $-1/2$ winding number defects [51], which is due to the backflow. Similar asymmetry was observed for the umbilic defects of strength $s = \pm 1$, where the $+1$ defects are again faster than the -1 [54].

Recently, the laser tweezers technique was used to control the creation of topological charges on and around a long, micrometer diameter glass fiber in a nematic liquid crystal [55,56]. Although a fiber is topologically equivalent to a sphere, both having the genus $g = 0$, there is a remarkable difference in the complexity of the topological defects on a microsphere and a fiber. Because of its elongated shape, many novel topological states become stable (or metastable) on a fiber, and these states are accessible by a rapid quenching of a section of a liquid crystal surrounding the fiber. This quench is induced by first locally heating the NLC into the isotropic phase by using light absorption of the laser tweezers, and then the light is switched off. A dense tangle of topological defects is created after the quench through a process similar to the Kibble-Zurek mechanism of topological monopoles formation [57–60]. Depending on the orientation of the fiber with respect to the overall NLC alignment in the measuring cell, different types and number of topological monopoles are in this way created and stabilized. These include the pairs of a Saturn ring and Saturn antiring, having opposite winding numbers, pairs of point monopoles with opposite topological charges, and many other interesting topological objects, such

as metastable zero-topological charge loops. Like a particle and its antiparticle in particle physics, these topological entities tend to attract and annihilate if let free. The annihilation of a pair of rings on the fiber has been analyzed recently [55], but other annihilation processes were left unexplored.

Here we focus on the process of creation and the dynamics of annihilation of a pair of topological point defects on a fiber, set perpendicularly to the overall NLC alignment. By cutting and moving defect loops on the fiber we are able to create in a fully controllable way a single pair of topological defects, i.e., a hyperbolic and a radial hedgehog, both positioned in the vicinity of the surface of the fiber and separated by several micrometers. We analyze the motion of these defects, as they are attracted by the elastically deformed director field around them and are sliding along the surface of the fiber towards each other until they annihilate. We compare our results to previous experiments on the annihilation of topological defects in NLCs.

II. EXPERIMENT

In our experiments we used glass fibers with diameters 8–12 μm, which were made by heating a commercially available 125-μm optical glass fibers with oxygen-hydrogen torch and mechanical stretching. The fibers were cleaned in an ultrasonic bath for 30 min, using a solution of water and detergent. Then fibers were cleaned off with detergent and rinsed several times with deionized water. The remaining organic material adsorbed to the surface of the fibers was removed by placing the fibers in an oxygen plasma (Tegal plasmaline 421) at 100 °C for 1 h. After plasma cleaning, the surface of the fibers was coated with a monolayer of N,N-dimethyl-N-octadecyl-3-aminopropyltrimethoxysilyl chloride (DMOAP) silane (ABCR GmbH) using a standard procedure. This monolayer ensures strong perpendicular surface anchoring of nematic liquid crystal 5CB, used in the experiments. The fiber from the tapered end was placed between two parallel optically transparent Indium Tin Oxide (ITO)-coated glass slides, covered with a thin layer of a rubbed polyimide (PI 5291, Brewer Science), which ensures an excellent planar LC alignment. The gap between glass plates was controlled with mylar spacers and was varied from 13 to 70 μm. The cell was glued with two component epoxy (UHU, GmbH, or Torr Seal, Varian). The cell thickness was measured by the interference method, using the spectrometer (USB2000, Ocean Optics). Then the fiber was cut from the tapered part to a length of 200–600 μm. By filling the cell with the LC, the microfiber moves inside the cell by capillary force of the LC flow. The ITO coating was used as an absorber of the laser light of the tweezers at the surface of the glass slides and provided very good control of the local heating of the LC. In this experiment, the long axes of fibers were oriented perpendicularly to the rubbing direction (i.e., the overall direction of LC molecules far from inclusions). In some of the experiments, silica microspheres 10 μm in diameter were immersed into the same cell. They were previously treated with the same silane to ensure the perpendicular surface alignment of the liquid crystal molecules. We used a laser-tweezers setup built around an inverted microscope (Nikon Eclipse, Ti-U) with an infrared 2-W fiber laser operating at 1064 nm as the light source and a pair of acousto-optic deflectors driven by a computerized system (Aresis, Tweez 70) for beam manipulation. The images were recorded using a Pixelink PLA 741 camera or a Canon EOS 550D camera at different frame rates from 10 to 100 fps.

III. RESULTS

A. Topological point monopoles on a fiber

When the fiber is set perpendicularly to the nematic director in a homogeneous and planar nematic cell with a cell gap of $\approx$20 μm, one observes a gigantic Saturn ring, encircling the fiber all along its length. An example of such a gigantic $-1/2$ ring is shown in the first panel of Fig. 1(a). The appearance of a single ring is not surprising and is the consequence of the conservation of the total topological charge in the system. Similarly to a spherical colloidal particle with homeotropic (perpendicular) surface anchoring of NLC molecules, which is encircled by a Saturn ring under appropriate surface or size conditions [61–63], a fiber must be encircled with a single Saturn ring, because the genus of the fiber and the microsphere are the same. The charge of the ring compensates the topological charge of the inserted fiber, which ruptures the director field and forces it to align along a closed surface. However, the surface of very long fiber is not so smooth as the surfaces of microspheres and the Saurn ring on the fiber is usually not so straight as the Saturn ring encircling a microsphere. Instead, one can see that the ring is formed of tens of micometers long zigzag sections, which are pinned to the impurities and protrusions on the fiber.

We have recently demonstrated how one can cut and shape individual topological monopoles (defects) out of this gigantic Saturn ring by using highly localized and strong beam of the laser tweezers [55,56]. We here briefly discuss the procedure of obtaining individual topological charges on a fiber, set perpendicularly to the nematic director, which is illustrated in Fig. 1.

The laser is focused to the vicinity of the fiber and the intensity of the light of the tweezers is set to the level, which causes local melting of the NLC into the isotropic phase. The isotropic island is clearly visible and has a sharp nematic-isotropic interface, which is a very strong attractor of particles and defects in NLC, as analyzed recently [25]. Using the interaction of this molten isotropic island with NLC texture, one can grab and cut the gigantic Saturn ring into individual sections, as shown in Fig. 1(a). Because of the conservation of the total topological charge of the gigantic Saturn ring, which is, by convention, equal to -1, each cutting of the ring must preserve the total topological charge. The first cut of the ring into two rings has a consequence that one of the rings preserves the charge of -1, whereas the second ring must be charge neutral. These charge-neutral rings have at least two sections, each of them having opposite winding number, which transform smoothly into one another through the topological soliton, as indicated in the last panel of Fig. 1(a) [55,56].

The second cut is executed on either side of the topological soliton. In Fig. 1(b), this was done on the right side of the soliton, where the loop had the winding number of $+1/2$. This cut creates a smaller loop on the right side of the soliton,

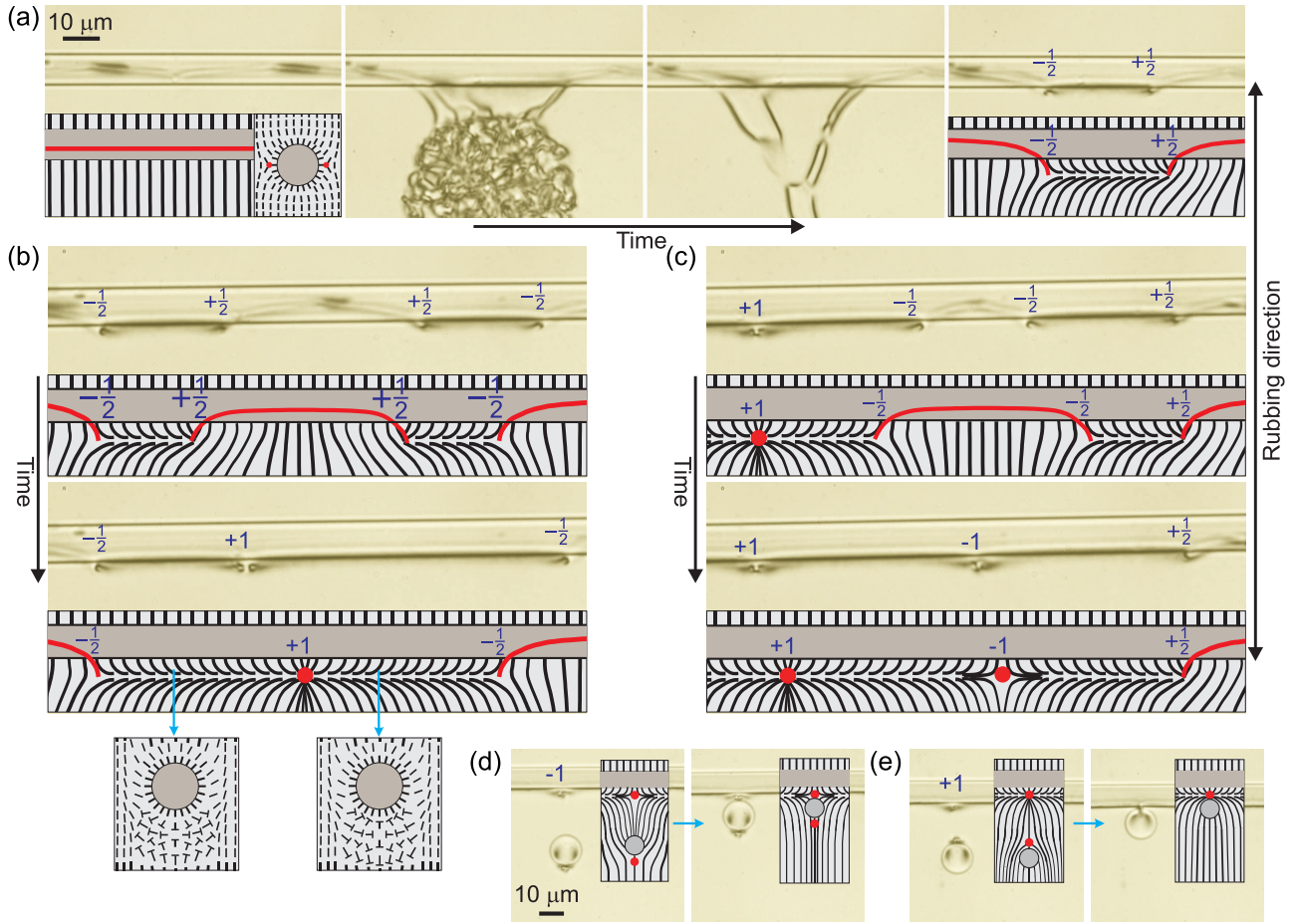

FIG. 1. (a) The microfiber is oriented perpendicularly to the nematic director in the planar cell, and a gigantic Saturn ring is spontaneously created that encircles the fiber along the long axis. Note that the ring is not straight but forms zigzag sections, because it is pinned to the surface impurities at different positions. This ring is cut by the laser tweezers into two separated rings with locally opposite winding numbers. The smooth region in between is called the "topological soliton." (b) When the ring on the right (assigned the $+1/2$ winding number) is cut again with the tweezers, a $+1/2$ loop is created, which shrinks into the $+1$ point defect. A $-1/2$ winding loop is left on the right side. (c) The same procedure of cutting is performed on the loop on the right side of this $+1$ defect. This creates a $-1/2$ winding number loop, which shrinks into a -1 point defect. [(d) and (e)] The charges of these point defects are tested by small dipolar colloidal particles. They bind to oppositely charged point defects in opposite orientation of their topological dipole.

which shrinks into a point monopole, touching the surface of the fiber. As shown in Figs. 1(d) and 1(e) its topological charge can be determined by using a test dipolar colloidal particle, which is attracted to this point defect either with its body or the hedgehog defect. When the body of the colloid is attracted to the monopole, the monopole has the -1 charge, because the body carries the $+1$ charge by definition. If the colloid is attracted to the point monopole with its hedgehog, carrying the -1 charge, the monopole is clearly carrying the $+1$ topological charge. From the view of topology, our system is a two-dimensional problem and the rules of attraction are rather simple: Equal charges repel, and opposite charges attract. This allows for reliable and consistent identification of the sign of the point topological charge. Additional monopoles can be created at will, as shown in Fig. 1(c). Due to the conservation of the topological charge, the sign of thus-created monopoles always alternates in successive steps. The strength of the interactions depends on the elastic deformation, where the 3D nature of the nematic director field around the fiber and colloids has to be considered.

By repeating the cutting procedure, an arbitrary number of topological monopoles can be created close to the fiber. They are elastically attracted to the fiber, because this position lowers their total elastic energy; they can slide along the fiber or can be moved with the laser tweezers along the fiber as well. An example of a sequence of topological point defects, alternating in the topological charge, are shown in Fig. 2(a). The charges of monopoles are identified by an interacting dipole, as illustrated in Fig. 2(b).

B. Annihilation of a hyperbolic and radial hedgehog on a fiber

Because the pairs of topological charges were created either from "vacuum" or by cutting topological defect lines, they tend to attract and mutually annihilate. There are attractive forces with elastic origin between the point monopoles, because of their opposite topological charges, say, because of the elastically distorted region of the NLC, connecting both defects. The monopoles can attract each other from very large separation (several 100 μm). They begin to visually overlap

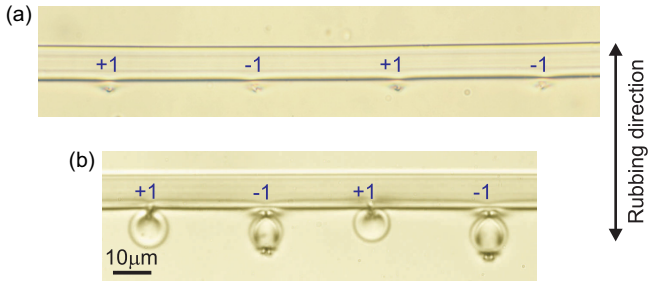

FIG. 2. Sequence of point monopoles with alternating charge. (a) A sequence of point monopoles are created on a fiber by cutting the gigantic Saturn-ring with laser tweezers. (b) The charge of monopoles are demonstrated by dipole.

when their separation is less than 10 μm. After touching each other, they annihilate similarly to the annihilation of the Saturn ring and Saturn antiring on the fiber, reported recently [55].

Figure 3(a) shows a typical time sequence of images of the attraction and annihilation of the pair of topological monopoles. The process of monopole annihilation is video recorded at a frame rate of 20 fps. From the stored images, the positions of both defects are determined from each recorded frame using particle-tracking software. This allows for a complete reconstruction of the trajectories of both defects in time with a resolution of ± 30 nm, as shown in Fig. 3(b). Here, the starting separation of both point defects was nearly 100 μm.

In the next step, we calculate the velocity of each point defect by applying the numerical derivative to each of the recorded trajectories. This calculated velocity enables us to determine the force acting on that defect. Namely, it is well known that the topological monopole-monopole interaction should follow universal power-law dependence of the force versus monopole separation [64]. It is also well accepted in the soft matter community that the elastic force between colloidal particles (and topological defects) can be determined from the equation of balance between the driving-elastic force and the viscous drag force [65], which was applied to many experiments on colloidal pair interactions. To determine the

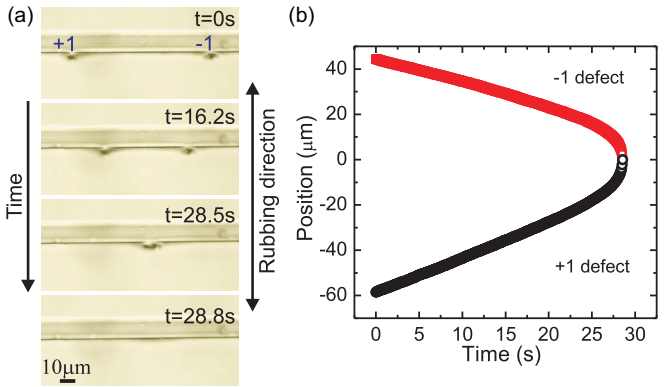

FIG. 3. Annihilation of point monopoles on a fiber from large starting separation. (a) The time sequence of images showing the annihilation of point monopoles. (b) The position of the $+1$ and -1 point monopoles as a function of time.

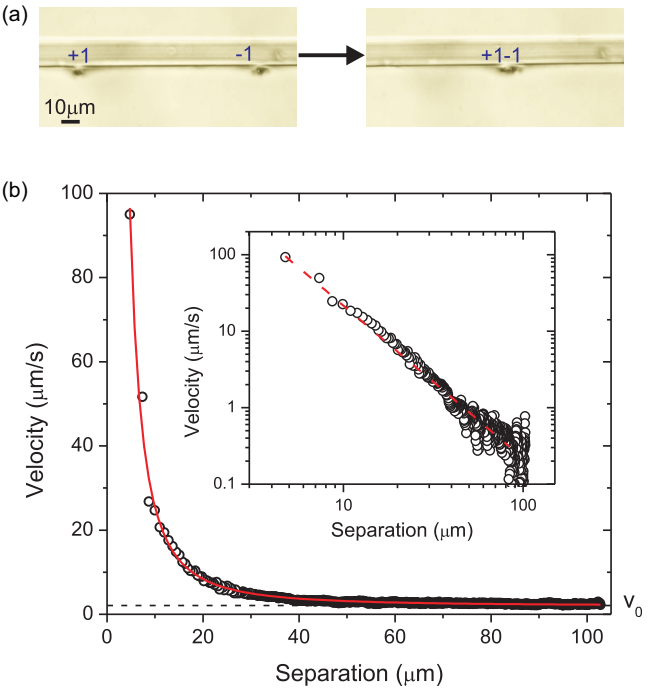

FIG. 4. Annihilation dynamics of two point monopoles, released from a large separation of $\approx$100 μm in a cell of 20-μm thickness. (a) The optical micrographs of point monopoles at starting and ending position just before annihilating each other. (b) Relative velocity of the monopoles versus their separation. At large separation, the monopoles are approaching each other with a constant velocity of $v_0 = 2.1$ μm/s. This means that the attractive force is constant. At small separations, the velocity and the attracting force show a power-law behavior. The red line shows power-law fit of the velocity as a function of separation $v(d) = v_0 + d^{-\alpha}$, with $\alpha = 2$. The inset shows the power-law fit of the velocity as a function of separation, when the background velocity v_0 is subtracted, yielding $\alpha = 2.0 \pm 0.2$.

separation dependence of the force one therefore needs to measure the viscous drag coefficient for a given particle or a defect. This is usually done by performing a separate experiment, where a Brownian motion of the colloidal particle or a defect is measured for sufficiently long time. From the recorded Brownian trajectory one can determine very precisely the real value of the viscous drag coefficient for a selected particle or defect. However, if one is not interested in real values of the interaction force between the two particles (or defects), but is interested only in their separation dependence, then it is sufficient to analyze the separation dependence of the relative velocity of the two interacting entities, because this is proportional to the interacting force.

We studied the dynamics of annihilation of a single pair of monopoles, which were well isolated from other defects or the ends of the fiber. By using the laser tweezers, the monopoles were moved apart to the starting separation of $\approx$100 μm, and then the monopoles were let free to interact. Figure 4 shows the dynamics of the monopoles' approach and annihilation. We find from seven experiments performed on three different fibers that the pair interacting force between two monopoles on the fiber has two characteristic regimes. In the far-field regime, when the monopoles are well separated from each other, they

always approach each other with a constant velocity. This constant velocity slightly differs for different experiments and ranges from 1.3–2.2 μm/s, whereas the average velocity for seven experiments is $v_0 = 1.7 \pm 0.4$ μm/s. The origin of this background constant velocity is in the inaccuracy in setting the fiber exactly perpendicular to the rubbing direction of the cell, as will be discussed later in this section. Constant far-field velocity means that the force pulling the two monopoles together is constant, i.e., independent of separation.

In the near-field regime, when the two monopoles start to overlap, the interaction force, which is pulling them together, starts to increase, as the monopoles approach each other. The velocity of approach (and therefore also the attractive pair interaction force) in Fig. 4 can indeed be described as a sum of two terms: (i) a constant velocity v_0, and (ii) the near-field pair-interaction force resulting in the power-law dependence of their relative velocity of approach $v \propto 1/d^{\alpha}$, with $\alpha \approx 2 \pm 0.2$, when the background velocity is subtracted [see the inset to Fig. 4(c)]. In all experiments we find similar behavior.

The constant background velocity v_0, which appears in the far-field region at separations more than $\approx$40 μm, is similar to previous observations of constant force attraction of surface boojums in a thin nematic layer with hybrid boundary conditions, first observed a long time ago by Lavrentovich and Rozhkov [43]. They observed "strings" with a boojum and an antiboojum at their ends, and the string contracted at constant velocity, which implies constant force of attraction, similarly to our observations. Similar string-like behavior and constant force of attraction was observed in other experiments [42,45].

The origin of constant force of attraction of two point monopoles on a fiber can be understood by considering the elastic deformation of the director field around each monopole, which is schematically shown in Fig. 5. Each monopole is surrounded by two regions of "escape," i.e., strongly deformed regions with splay-bend deformation, also called topological solitons. These regions are propagating the topological flux between neighboring monopoles and are nonsingular, i.e., smooth. Because of the elastic deformation, each of these soliton regions presents an elastic string which is pulling the point defect in a direction which minimizes its elastic energy. However, because the elastic energy is proportional to the length of the soliton region, the stringlike force of each of these soliton regions is constant, i.e., independent of the length of the escape region. This leads to a conclusion that the total force on each monopole, shown schematically in Fig. 5(a) should be zero, because the string force pulling the defect to the left cancels the string force pulling it to the right and the monopoles should not interact with each other. This is in clear contradiction with our experiments, which always show an attractive and constant far-field force between the two monopoles. However, there is a very important detail missing here: We see from many experiments performed that this background far-field constant interaction force differs in different experiments.

The answer to this observation is in the limited precision in setting the fiber exactly perpendicular to the rubbing direction of the cell, which determines the undisturbed nematic director in our experimental cells. Namely, if there is any offset in the orientation of the fiber from this 90° angle, the topological solitons on each side of the monopoles will be no longer equal,

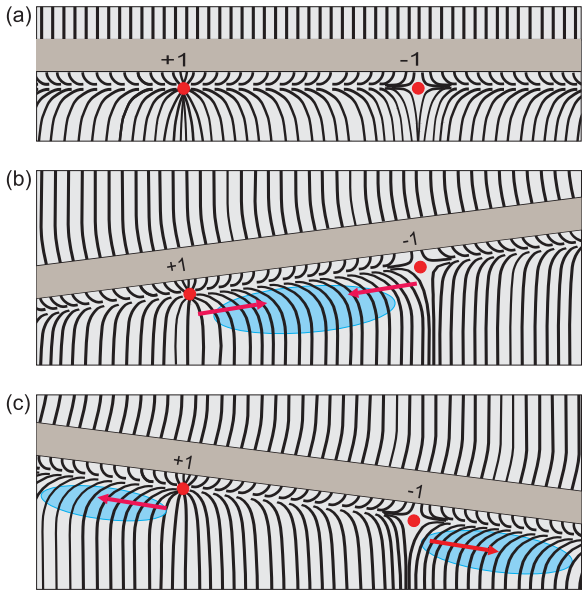

FIG. 5. Schematic representation of the director around the fiber at different angles with respect to the far-field nematic director. (a) The fiber is set perpendicularly to the nematic director. The monopoles are stable in the far-field region, because the force to the left is balanced with the force to the right. (b) The fiber is rotated counterclockwise. The monopoles start to move towards each other with constant velocity to diminish the energetically costly region. (c) The fiber is rotated clockwise. The monopoles are moving away from each to reduce the region with high elastic energy.

as illustrated in Figs. 5(b) and 5(c). Figure 5(b) illustrates what happens to the elastically deformed soliton region when the fiber is rotated counterclockwise. Some regions of elastic distortion become even more distorted, as illustrated by the shaded region in Fig. 5(b). On the other hand, neighboring solitons become less distorted. Because of a higher elastic distortion, a structural force is generated, which tends to minimize this energetically high-cost region, and the two monopoles are pulled together to shorten the length of this unfavorable soliton. The interaction between the monopoles is in this case attractive.

An opposite behavior is expected, when the fiber is rotated clockwise, as shown in Fig. 5(c). One can immediately recognize a difference between the two topological solitons, and the far-field interaction between two oppositely charged monopoles is repulsive and the monopoles should start to move away from each other to reduce the energy and the pair-interaction force.

It is exactly this behavior that we observe in the experiments, and the observation of a repulsive force between two oppositely charged topological monopoles was in fact a crucial clue for figuring out the mechanism of the far-field interaction force between two monopoles on a fiber. Figures 6(a) and 6(b) show selected video snapshots of two experiments, where the monopoles start to move towards each other or away from each other, depending on the direction of the rotation of the fiber with respect to the rubbing direction. When the fiber is rotated counterclockwise, the far-field pair-interacting force between the monopoles is attractive. In this case the monopoles

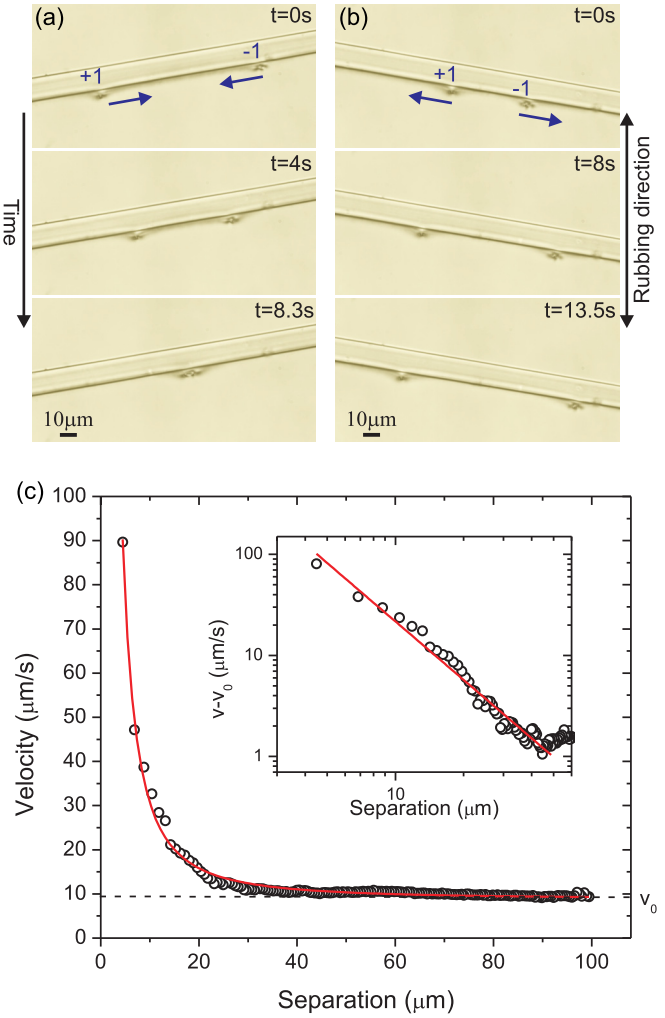

FIG. 6. Attraction and repulsion of oppositely charged topological monopoles on a fiber, depending on the sign of rotation of the fiber with respect to the cell director. (a) Attraction of the monopoles on the fiber, which was rotated counterclockwise. (b) The two oppositely charged monopoles repel each other when the fiber is rotated clockwise with respect to the cell director. The cell thickness is 20 μm. (c) The relative velocity of the monopoles versus their separation in case (a) has a constant value in the far field. It increases at smaller separation of the two monopoles, where it shows a power-law dependence. The red line shows power-law fit of the velocity as a function of separation $v(d) = v_0 + d^{-\alpha}$, with $v_0 = 10$ μm/s and $\alpha = 2$. The inset shows the power-law fit of the velocity as a function of separation, when the background velocity v_0 is subtracted, yielding $\alpha = 2.0 \pm 0.2$.

are moving towards each other with the constant velocity of $v_0 = 10$ μm/s. On the contrary, when the fiber is rotated clockwise with respect to the director, the pair-interacting force is repulsive and the defects move away from each other, as shown in Fig. 6(b).

From the performed experiments we find that even a small inaccuracy in setting the angle between the fiber and the bulk orientation of the NLC to exactly 90° is the reason for the observed far-field attraction force and background velocity v_0. To test this hypothesis, we performed a series of experiments, where the fiber was rotated for a given angle with respect to the

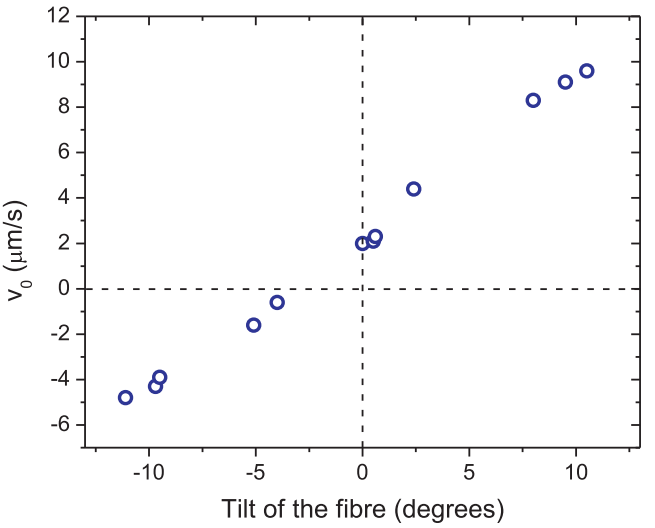

FIG. 7. Attraction and repulsion of opposite monopoles on a fiber as a function of the angle of rotation of the fiber with respect to the cell director. Negative velocity denotes repulsion, and positive velocity denotes attraction. The experiments were performed in a cell of 20-μm thickness.

cell director, and the background velocity v_0 was measured for each angle. Figure 7 shows the far-field constant velocity v_0 of the two monopoles on the fiber versus the angle of rotation of the fiber with respect to the cell director. The relation is close to linear but is not symmetric around the zero angle. This is due to inaccuracy in the absolute determination of the cell director under the microscope. The experiment on monopole annihilation on a fiber in a nematic liquid crystal is therefore very sensitive to the precision of the mechanical alignment of the fiber with respect to the director orientation in the measuring cell. Even a small deviation of the fiber orientation for a few degrees from the perpendicular direction to the director will result in significant background velocity of the monopoles of several μm/s.

IV. DISCUSSION

Our experiments on the annihilation of hedgehog monopoles on the fiber demonstrate two different regimes of monopole interaction, which is in accordance with previous observations. At large separation, the hedgehogs are attracted by a stringlike constant force, which is similar to surface boojums annihilation in hybrid nematic films studied by Lavrentovich and Rozhkov [43] and Rapini *et al.* [44]. At small separation, this constant force transforms into the separation-dependent attractive force, also observed and analyzed in a number of experiments. Pargellis *et al.* [42] analyzed the annihilation of point monopoles in cylindrical capillaries filled with the nematic liquid crystal, which were first studied by Williams *et al.* [53]. A cylindrical geometry with perpendicular surface anchoring is a very elegant experimental setting for creation and annihilation of monopoles in the NLC. Using a thermal or pressure quench, they observed two distinct dynamical regimes of monopole attraction and annihilation. At early times, when the monopoles are well separated by a distance much larger than the diameter of the capillary, the

separation between the monopoles decreased linearly with time and the velocity of mutual approach was constant. This was followed by a crossover into the square-root dependence of the separation d versus the time t, $d \propto (t_\circ - t)^{0.5}$ over nearly 3 decades.

Quite similar dynamical regimes were observed by Bogi *et al.* [46] for the annihilation of $+1/2$ and $-1/2$ disclination lines in planar nematic cells. At large separation, the velocity of mutual approach is constant and the separation decreases linearly with time. At closer separation, mutual elastic interaction of the profiles of both disclination lines takes place and the regime is nonlinear, but the power-law dependence could not be resolved in the experiments. In this regime, the monopoles move faster and their velocity of approach increases with respect to the far-field constant velocity. Similar crossover in the dynamics of mutual attraction was observed by Minoura *et al.* [45] for the annihilation of wedge disclination pair. Again, a linear regime with a constant velocity of attraction was observed at a larger separation, whereas at a closer separation a crossover to a square-root time dependence, $d \propto (t_\circ - t)^{0.5}$, was observed, as t tends to the time of collision $t_\circ$.

In the far-field regime, our findings are consistent with other experiments on monopole-antimonopole annihilation, because we also observe attraction with constant velocity. Whereas in other experiments constant velocity of attraction is caused by disclination loop, it is caused by the tilt of the fiber and the asymmetry of the escape soliton between the monopoles in our experiments.

The analysis of the monopole-monopole interaction in the near field regime is quite delicate, because of the constant velocity background present in all our experiments. In the analysis of the near-field interaction, we subtracted this background velocity and then analyzed the remaining increase of the velocity when the monopoles are approaching towards the point of annihilation. The subtraction of the background velocity is justified in our experiments, because the reason for this background velocity is the tilt of the fiber. It can be seen from the insets to Fig. 5(c) and Fig. 6(c) that the remaining change of the velocity in the near field shows clear power-law dependence on the monopole separation with the exponent $\alpha = 2.0 \pm 0.2$.

This near-field power-law behavior of the monopole velocity during attraction, $v \propto 1/d^2$, is a strong indication of a Coulomb-like force between the two point monopoles, where the elastic attractive force $F_{\rm mon}$ between topological monopole, $F_{\rm mon} \propto 1/d^2$. The Coulomb-like attractive near field force between point hedgehogs can be expected following the arguments of Minoura *et al.* [45]. The deformation of the director field is governed by the Laplace equation, which means that the elastic force between two elastic monopoles should follow the general $1/r^2$ dependence for all types of monopoles, governed by the Laplace equation. Similarly, the elastic force between two elastic dipoles should scale as $F_{\rm dip} \propto 1/d^4$ and the pair quadrupolar force as $F_{\rm quad} \propto 1/d^6$. These power laws were actually experimentally confirmed for elastic dipoles and quadrupoles. In those kind of measurements, one measures the velocity of the multipoles when approaching each other. During this approach the Stokes drag force due to the motion of the multipole through a viscous liquid crystal is balanced at all times with the multipole interaction force.

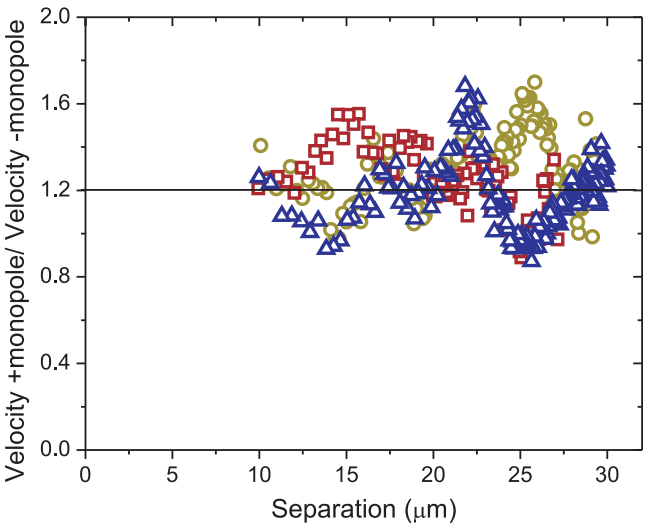

FIG. 8. Ratio of the velocities of the $+1$ and -1 point monopole during their annihilation on a fiber in a cell of 20-μm thickness. The ratios are plotted for three different samples. The average value of $v_+/v_- \approx 1.2$.

The Stokes drag force is measured in a separate experiment, which is following and tracking the Brownian motion of these multipoles.

In our experiments, it is impossible to determine strictly the force between the two monopoles, because we cannot determine the viscosity coefficient and follow its change during the monopole interaction. If we consider that the viscosity coefficient is simply given by Stokes's law, and is constant for all separations between the monopoles, then the monopole interaction is given by Coulomb's law. However, we have no direct evidence that the viscosity coefficient is constant, especially for close separations, when the two regions of elastic distrotion of both monopoles start to overlap.

We have observed a similar power-law dependence with $\alpha \approx 2.2$ in our previous work [55], where the annihilation of two Saturn rings was observed. In that experiment there was no constant velocity at large separation because of different geometry. The fiber was parallel to the nematic director and there was no topological soliton between the Saturn rings, which could eventually cause the stringlike attraction.

Finally, we have to mention that in all experiments performed, the $+1$ monopole is always faster than the -1 monopole, and the ratio of their velocities is $v_+/v_- \approx 1.2$. This is shown in Fig. 8 for three different samples. Most likely, this is due to their different hydrodynamic properties, as discussed in many experiments reported so far, which consistently reported faster movement of the $+$ defects [47,50,54].

V. CONCLUSIONS

Our experiments on the dynamics of annihilation of point monopoles on a fiber reveal that there is a crossover in the pair-interaction force at a certain monopole separation, which is, in our case, around 40 μm. In the experiments we have measured relative velocity of monopoles which is proportional to the interacting force. For larger separations, the force between the monopoles is independent of separation and results in

a constant velocity of approach. For smaller separation, the attractive force increases with decreasing separation d, resulting in velocity scaling as $v \propto 1/d^2$. Most interestingly, the far-field force may be either attractive or repulsive, even for oppositely charged monopoles, which is quite counterintuitive. This is explained in terms of experimental inaccuracy in setting the fiber exactly perpendicular to the cell director and appears to be a technical problem of these experiments. It is actually quite difficult to fix the fiber completely perpendicularly to the rubbing direction, because the torque of the liquid crystal tries to rotate the fiber along the director in the cell. This misalignment has a strong affect on the far-field interaction of the point monopoles.

In conclusion, the experiments on the interaction of topological monopoles on a fiber show us that this experimental setting provides an interesting environment for the creation, manipulation, and analysis of topological defects. We have shown that the relative velocity of monopoles during the near-field interaction is proportional to the inverse square of their separation, which is a strong indication that the interacting force between elastic monopoles follows the Coulomb law for electric monopoles $F \propto (1/d)^2$. One could envisage further experiments with curved and deformed fibers in chiral nematic liquid crystals, where the richness of possible topological states is expected to increase. This increased topological complexity requires new experimental techniques for the analysis of director fields, such as fluorescent confocal microscopy, supported by reliable numerical technique for 3D director reconstruction. It remains to be demonstrated in future experiments.

ACKNOWLEDGMENTS

This work was supported by the European Commission Marie Curie project HIERARCHY Grant No. PITN-GA-2008-215851 (M.N.) and the Slovenian Research Agency (ARRS) contracts P1-0099 and J1-6723 (M.Š. and I.M.). The authors thank Simon Čopar for helpful discussion.

[1] Y. Bouligand, J. Phys. (Paris) **35**, 215 (1974).
[2] P. G. de Gennes and J. Prost, *The Physics of Liquid Crystals* (Oxford Science, Oxford, 1993).
[3] P. M. Chaikin and T. C. Lubensky, *Principles of Condensed Matter Physics* (Cambridge University Press, New York, 1995).
[4] N. D. Mermin, Rev. Mod. Phys. **51**, 591 (1979).
[5] M. V. Kurik and O. D. Lavrentovich, Usp. Fiz. Nauk **154**, 381 (1988).
[6] M. Kleman, Rep. Prog. Phys. **52**, 555 (1989).
[7] O. D. Lavrentovich, Liq. Cryst. **24**, 117 (1998).
[8] G. E. Volovik and V. P. Mineev, Sov. Phys. JETP **45**, 1186 (1977).
[9] R. Pratibha and N. V. Madhusudana, Mol. Cryst. Liq. Cryst. **198**, 215 (1991).
[10] P. Poulin, H. Stark, T. C. Lubensky, and D. A. Weitz, Science **275**, 1770 (1997).
[11] Jun-ichi Hotta, K. Sasaki, and H. Masuhara, Appl. Phys. Lett. **71**, 2085 (1997).
[12] S. Juodkazis, M. Iwashita, T. Takahashi, S. Matsuo, and H. Misawa, Appl. Phys. Lett. **74**, 3627 (1999).
[13] S. Juodkazis, S. Matsuo, N. Murazawa, I. Hasegawa, and H. Misawa, Appl. Phys. Lett. **82**, 4657 (2003).
[14] T. A. Wood, H. F. Gleeson, M. R. Dickinson, and A. J. Wright, Appl. Phys. Lett. **84**, 4292 (2004).
[15] H. F. Gleeson, T. A. Wood, and M. Dickinson, Phil. Trans. R. Soc. A **364**, 2789 (2006).
[16] Y. Iwashita and H. Tanaka, Phys. Rev. Lett. **90**, 045501 (2003).
[17] M. Yada, J. Yamamoto, and H. Yokoyama, Phys. Rev. Lett. **92**, 185501 (2004).
[18] I. Muševič, M. Škarabot, D. Babič, N. Osterman, I. Poberaj, V. Nazarenko, and A. Nych, Phys. Rev. Lett. **93**, 187801 (2004).
[19] I. I. Smalyukh, A. N. Kuzmin, A. V. Kachynski, P. N. Prasad, and O. D. Lavrentovich, Appl. Phys. Lett. **86**, 021913 (2005).
[20] M. Škarabot, M. Ravnik, D. Babič, N. Osterman, I. Poberaj, S. Žumer, I. Muševič, A. Nych, U. Ognysta, and V. Nazarenko, Phys. Rev. E **73**, 021705 (2006).
[21] B. Lev, A. Nych, U. Ognysta, S. B. Chernyshuk, V. Nazarenko, M. Škarabot, I. Poberaj, D. Babi, N. Osterman, and I. Muševič, Eur. Phys. J. E **20**, 215 (2006).
[22] J. Kotar, M. Vilfan, N. Osterman, D. Babič, M. Čopič, and I. Poberaj, Phys. Rev. Lett. **96**, 207801 (2006).
[23] I. Smalyukh, A. V. Kachynski, A. N. Kuzmin, and P. N. Prasad, Proc. Natl. Acad. Sci. U.S.A. **103**, 18048 (2006).
[24] L. Lucchetti, L. Criante, F. Bracalente, F. Aieta, and F. Simoni, Phys. Rev. E **84**, 021702 (2011).
[25] M. Škarabot, Ž. Lokar, and I. Muševič, Phys. Rev. E **87**, 062501 (2013).
[26] I. I. Smalyukh1, S. V. Shiyanovskii, and O. D. Lavrentovich, Chem. Phys. Lett. **336**, 88 (2001).
[27] I. I. Smalyukh *et al.*, Mol. Cryst. Liq. Cryst. **450**, 79 (2006).
[28] I. I. Smalyukh and O. D. Lavrentovich, Phys. Rev. E **66**, 051703 (2002).
[29] I. Muševič, M. Škarabot, U. Tkalec, M. Ravnik, and S. Žumer, Science **313**, 954 (2006).
[30] M. Škarabot, M. Ravnik, S. Žumer, U. Tkalec, I. Poberaj, D. Babič, N. Osterman, and I. Muševič, Phys. Rev. E **76**, 051406 (2007).
[31] M. Škarabot, M. Ravnik, S. Žumer, U. Tkalec, I. Poberaj, D. Babič, N. Osterman, and I. Muševič, Phys. Rev. E **77**, 031705 (2008).
[32] A. B. Nych, U. M. Ognysta, V. M. Pergamenshchik, B. I. Lev, V. G. Nazarenko, I. Muševič, M. Škarabot, and O. D. Lavrentovich, Phys. Rev. Lett. **98**, 057801 (2007).
[33] I. Muševič and M. Škarabot, Soft Matter **4**, 195 (2008).
[34] U. Ognysta, A. Nych, V. Nazarenko, I. Muševič, M. Škarabot, M. Ravnik, S. Žumer, I. Poberaj, and D. Babič, Phys. Rev. Lett. **100**, 217803 (2008).
[35] A. Nych, U. Ognysta, M. Škarabot, M. Ravnik, S. Žumer, and I. Muševič, Nat. Commun. **4**, 1489 (2013).
[36] M. Ravnik, M. Škarabot, S. Žumer, U. Tkalec, I. Poberaj, D. Babič, N. Osterman, and I. Muševič, Phys. Rev. Lett. **99**, 247801 (2007).

[37] U. Tkalec, M. Ravnik, S. Čopar, S. Žumer, and I. Muševič, Science **333**, 62 (2011).
[38] V. S. R. Jampani, M. Škarabot, M. Ravnik, S. Čopar, S. Žumer, and I. Muševič, Phys. Rev. E **84**, 031703 (2011).
[39] I. I. Smalyukh, Y. Lansac, N. A. Clark, and R. P. Trivedi, Nat. Mater. **9**, 139 (2010).
[40] Bryan Gin-ge Chen, P. J. Ackerman, G. P. Alexander, R. D. Kamien, and I. I. Smalyukh, Phys. Rev. Lett. **110**, 237801 (2013).
[41] P. E. Cladis, W. van Saarloos, P. L. Finn, and A. R. Kortan, Phys. Rev. Lett. **58**, 222 (1987).
[42] A. Pargellis, N. Turok, and B. Yurke, Phys. Rev. Lett. **67**, 1570 (1991).
[43] O. D. Lavrentovich and S. S. Rozhkov, JETP Lett. **47**, 254 (1988).
[44] A. Rapini, L. Leger, and A. Martinet, J. Phys. (Paris) Colloq. **36**, C1-189 (1975).
[45] K. Minoura, Y. Kimura, K. Ito, R. Hayakawa, and T. Miura, Phys. Rev. E **58**, 643 (1998).
[46] A. Bogi, P. Martinot-Lagarde, I. Dozov, and M. Nobili, Phys. Rev. Lett. **89**, 225501 (2002).
[47] C. Blanc, D. Svenšek, S. Žumer, and M. Nobili, Phys. Rev. Lett. **95**, 097802 (2005).
[48] T. Yanagimachi, S. Yasuzuka, Y. Yamamura, and K. Saito, J. Phys. Soc. Jpn. **81**, 034601 (2012).
[49] C. Denniston, Phys. Rev. B **54**, 6272 (1996).
[50] G. Toth, C. Denniston, and J. M. Yeomans, Phys. Rev. Lett. **88**, 105504 (2002).
[51] D. Svenšek and S. Žumer, Phys. Rev. E **66**, 021712 (2002).
[52] C. Liu, J. Shen, and X. Yang, Commun. Comput. Phys. **2**, 1184 (2007).
[53] C. Williams, P. Pieranski, and P. E. Cladis, Phys. Rev. Lett. **29**, 90 (1972).
[54] I. Dierking, M. Ravnik, E. Lark, J. Healey, G. P. Alexander, and J. M. Yeomans, Phys. Rev. E **85**, 021703 (2012).
[55] M. Nikkhou, M. Škarabot, S. Čopar, M. Ravnik, S. Žumer, and I. Muševič, Nat. Phys. **11**, 183 (2015).
[56] M. Nikkhou, M. Škarabot, and I. Muševič, Eur. Phys. J. E **38**, 23 (2015).
[57] W. H. Zurek, Phys. Rep. **276**, 177 (1996).
[58] B. van Heck, M. Burrello, A. Yacoby, and A. R. Akhmerov, Phys. Rev. Lett. **110**, 086803 (2013).
[59] I. Chuang, R. Durrer, N. Turok, and B. Yurke, Science **251**, 1336 (1991).
[60] J.-i. Fukuda and H. Yokoyama, Phys. Rev. Lett. **94**, 148301 (2005).
[61] E. M. Terentjev, Phys. Rev. E **51**, 1330 (1995).
[62] O. Mondain-Monval, J. C. Dedieu, T. Gulik-Krzywicki, and P. Poulin, Eur. Phys. J. B **12**, 167 (1999).
[63] Y. Gu and N. L. Abbott, Phys. Rev. Lett. **85**, 4719 (2000).
[64] O. M. Tovkach, S. B. Chernyshuk, and B. I. Lev, Phys. Rev. E **86**, 061703 (2012).
[65] J. C. Loudet, P. Hanusse, and P. Poulin, Science **306**, 1525 (2004).